In Silico Assessment of a Multipore Electrode Design for High Power Short Duration Ablation

Argyrios Petras[1], Massimiliano Leoni[1], Zoraida Moreno Weidmann[2], Jose M Guerra[2], Luca Gerardo-Giorda[1,3]

[1] Johann Radon Institute for Computational and Applied Mathematics (RICAM), Austrian Academy of Sciences, Linz, Austria
[2] Department of Cardiology, Hospital de la Santa Creu i Sant Pau, IIB Sant Pau, Universitat Autònoma de Barcelona, CIBER CV, Barcelona, Spain
[3] Institute for Mathematical Methods in Medicine and Data-Based Modelling, Johannes Kepler University, Linz, Austria

Abstract

High Power Short Duration (HPSD) ablation is an emerging approach to the radiofrequency catheter ablation for the treatment of cardiac arrhythmias. New catheter technologies have been introduced accommodating HPSD protocols, featuring multiple pores distributed around the electrode tip among others. Our previous in-silico assessment considered 6-pores electrodes, which were proven to not provide adequate cooling of the blood during the ablation. In this work, we explore the impact of a better electrode cooling system on the HPSD procedure using our previously validated computational model. A new electrode design is considered that consists of 66 irrigation pores based on state-of-the-art catheters used for HPSD. Ablations of 90W applied power for a duration of 4s for different contact forces show improved cooling of the electrode, without any steam pop complications. Yet, multiple pores around the electrode tip are not sufficient for effective blood cooling at low flows.

1. Introduction

Radiofrequency ablation using open-irrigated catheters is a commonly used treatment for cardiac arrhythmias. Recently, high-power short-duration ablation protocols have been introduced to increase the efficiency and reduce the duration of the procedure. These protocols use applied powers between 70-90W for 4-8s to eliminate the arrhythmogenic tissue. Typical state-of-the-art catheters that support these ablation protocols use an enhanced cooling system with multiple irrigation pores at the electrode tip. A previous study from our group indicated that catheters with 6 irrigation pores appear to be more prone to charring formation, reaching systematically temperatures higher than 80^oC in the blood [1]. This complication has been observed regardless of the shape of the electrode tip, hinting the need for better tip cooling systems.

In this study, we assess the effect of the presence of multiple irrigation pores at the electrode tip using our in-silico framework [2] on a simulated human atrial tissue.

2. Methods

2.1. Geometry

The simulation geometry is based on the in-vitro experimental setup [3] and consists of the blood chamber 80x80x54mm, the atrial tissue 80x80x6mm and a board that models the external factors of the system 80x80x20mm. The electrode, inspired from state-of-the-art catheters, has a diameter of 2.5mm and a length of 3.5mm. It consists of 66 irrigation pores of 0.116mm diameter spread around the electrode tip as shown in Fig. 1. Six cylinders of diameter 0.28mm are placed within the tip, mimicking 3 thermocouples and 3 mini electrodes. The design of the entire geometry and the electrode is shown in Fig. 1.

The mechanical interaction of the electrode with the tissue is described by the axisymmetric Boussinesq equation for a cylindrical profile with rounded corners [4], and the resulting deformation is applied to the tissue geometry.

2.2. Mathematical model

The interaction of the blood and the irrigated saline is described by the incompressible Navier-Stokes equations in the blood-saline subdomain. The electrical potential is governed by a quasi-static equation augmented with a con-
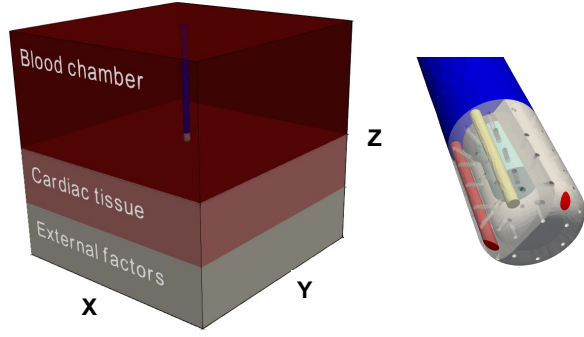
Figure 1. The computational domain (left) and the catheter tip design (right): the electrode (gray), the thermocouples (in yellow) and the minielectrodes (in red).

straint for constant power ablation in the whole computational domain. The temperature changes are modelled using a modified version of Penne's bioheat equation in the entire domain. The full system of equations is given in (1).

$$
\begin{aligned}
\frac{\partial \vec{v}}{\partial t} + \vec{v} \cdot \nabla \vec{v} - \mathbf{div}\, \mathbf{T}(\vec{v}, p) &= \vec{0}, \\
\mathbf{div}\, \vec{v} &= 0, \\
\rho c(T)\left(\frac{\partial T}{\partial t} + \vec{v} \cdot \nabla T\right) - \mathbf{div}(k(T)\nabla T) &= \sigma(T)|\nabla \Phi|^2, \\
\mathbf{div}(\sigma(T)\nabla \Phi) &= 0, \qquad (1) \\
\int_\Omega \sigma(T)|\nabla \Phi|^2 dx &= P_\Omega.
\end{aligned}
$$

In (1), $\vec{v}$ is the velocity, t is the time, $\mathbf{T}(\cdot, \cdot)$ is the stress tensor, p is the pressure scaled by the density, ρ is the density, $c(\cdot)$ is the temperature dependent specific heat, T is the temperature, $k(\cdot)$ and $\sigma(\cdot)$ are the temperature dependent thermal and electrical conductivities, Φ is the electrical potential, Ω is the computational domain and P_Ω is the power dissipated in Ω. More details on the model can be found in [2].

2.3. Boundary conditions

The blood inflow is imposed on one side of the blood chamber with the corresponding outflow zero pressure condition on the opposite side. The saline inflow is considered through the annular boundary at the top of the irrigation channel. No slip conditions are imposed at all the remaining boundaries.

A potential that satisfies the constant power constraint is imposed at the top surface of the electrode with the corresponding zero voltage at the bottom of the external effects board. No flux boundary conditions are applied at all the remaining boundaries of the domain.

A saline temperature is imposed at the annular boundary at the top of the irrigation channel and constant body temperature is considered at all external sides of the computational box. No thermal flux conditions are imposed lateral to the catheter body and at the top surfaces of the electrode, the thermocouples and the minielectrodes.

2.4. Model parameters

The model parameters are considered as in [1, 5]. Both the microelectrodes (ME) and the thermocouples (TC) are considered to be coated by a resistive material such as glass fiber, and thus are homogenized and modelled with the parameters of the thermistor as in [2]. Table 1 summarizes the values of the density ρ in kg/m^3, the specific heat c_1 in $J/(kgK)$, the electrical conductivity σ_0 in S/m and the thermal conductivity k_0 in $W/(mK)$ for the different subdomains of the model.

Table 1. The biophysical parameters of the model.

	Blood	Tissue	Board	Electrode	TC & ME
ρ	1050	1081	1076	21500	32
c_0	3617	3686	3017	132	835
σ_0	0.748	0.281	σ_b	4.6×10^6	10^{-5}
k_0	0.52	0.56	0.518	71	0.038

A linear temperature dependence is considered for the tissue specific heat, electrical and thermal conductivities as:

$$
\begin{aligned}
c(T) &= c_0\Big(1 - 0.0011(T - T_b)\Big), \\
\sigma(T) &= \sigma_0\Big(1 + 0.015(T - T_b)\Big), \\
k(T) &= k_0\Big(1 + 0.0022(T - T_b)\Big),
\end{aligned}
$$

where $T_b = 37^oC$ is the body temperature. The electrical conductivity of the external effects board σ_b is tuned to match the initial resistance of the system and power delivered to the tissue. Denoting with A the ratio of the electrode surface area in contact with the blood over the one with the tissue, and with Σ the corresponding ratio of the electrical conductivity, the power dissipated in the tissue is written as

$$
P_t = \frac{1}{1 + A\Sigma}P,
$$

where P is the total power given by the ablation protocol [2].

The mechanical properties of the simulated human atrial tissue are considered as in [6], with a Young's modulus of $40 kPa$ and Poisson's ratio of 0.499.

2.5. Lesion estimation

To provide a fair comparison against the simulated lesions with the 6-pore catheters [1], we consider the 50^oC

isotherm contour for the lesion size estimation. The measured quantities in this study include the lesion depth (D) from the undeformed tissue and width (W), as identified therein.

3.   Results

The system (1) is numerically solved using the finite element method, implemented in the FEniCSx computing platform (`fenicsproject.org`). The simulations were run in the in-house HPC cluster of RICAM.

We consider a high power protocol of $90W$ for a total of $4s$. The model simulates a total of $7s$: the saline irrigation is set to a standby mode of $2mL/min$ for $1s$, followed by an irrigation of $8mL/min$ for $2s$ before the beginning of the ablation [7]. The saline temperature is set to 22^oC, similar to [1].

The initial transition phase from standby mode to active irrigation allows for a better cooling of the electrode tip before the beginning of the ablation. Fig. 2 shows the effect on the cooling for different blood flow rates using a contact force of $10g$.

Next, we explore the complication rate of this electrode design for different contact forces ranging from $5g$ to $20g$. Table 2 shows the virtual ablation outcome for different blood flow velocities. The flow velocities were chosen to mimic the ones found in epicardium ($0m/s$), healthy atria ($0.1m/s$) and cavo-tricuspid annulus ($0.5m/s$) [1], and are also typical in in-vitro experimental setups [3]. The catheter provides safe ablations for high blood flow velocity of $0.5m/s$ and any chosen contact force. On the other hand, only for $5g$ and a low blood flow setting of $0.1m/s$ we get a safe ablation. The rest of the ablations with low and no blood flow resulted in the overheating of the blood at 80^oC, hence a charring complication. No steam pops were observed in the simulated ablations.

Table 2.   The list of complications for different contact forces and blood flow velocities. The green S indicates a safe protocol, while the yellow C the risk of charring formation.

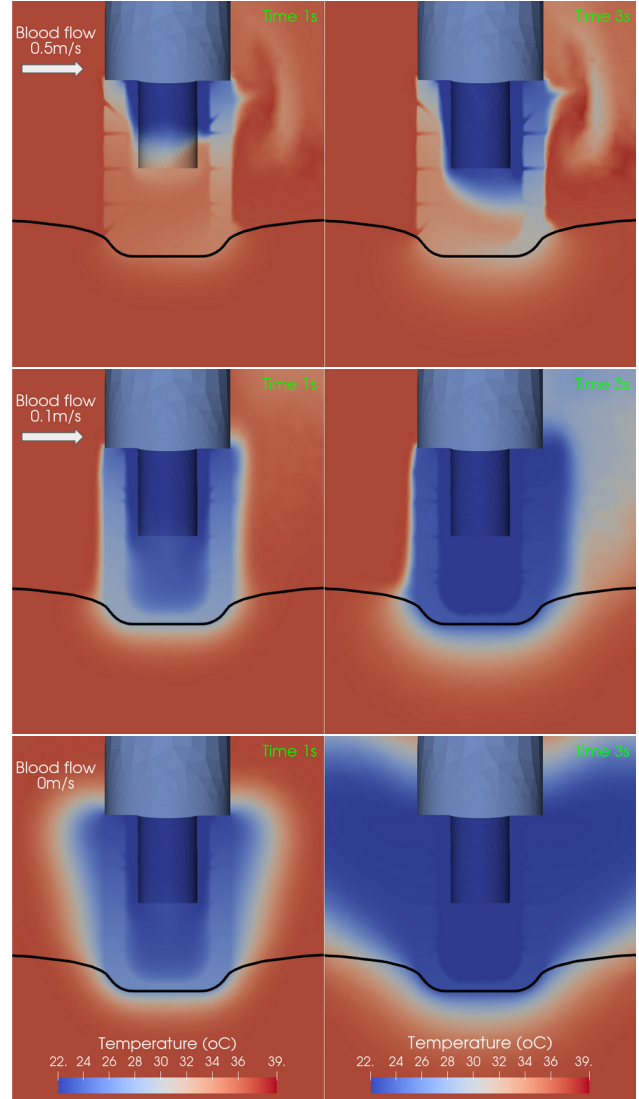| Force \ Blood flow	0.5 m/s	0.1 m/s	0 m/s
5g	S	S	C
10g	S	C	C
15g	S	C	C
20g	S	C	C

Figure 2.   The tip temperature for different blood flow at standby irrigation of $2mL/min$ (left, at $1s$) and right before the beginning of the ablation with $8mL/min$ (right, at $3s$).

Finally, using the high blood flow, at which no complications are observed, we explore the resulting lesion size dimensions for contact forces of $5 - 20g$. The resulting tissue temperature distribution and the lesion depth and width appear in Fig. 3. The lesion dimensions range between $5.2 - 7mm$ for the width and $2.6 - 4mm$ for the depth, as measured from the undeformed tissue. These values are comparable to the ones reported in the literature [8] for a total delivered energy of $360J$ using high power ablation protocols.
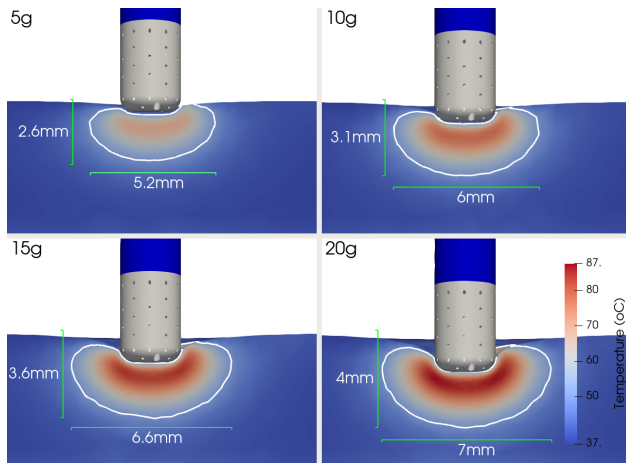
Figure 3. The tissue temperature distribution and lesion depth and width for contact forces of $5 - 20g$. The depth is measured from the undeformed tissue.

4.   Conclusions

The multipore electrode of this study appears to better cool the electrode and the surrounding blood when compared with the 6-pore electrodes. Yet for low and no blood flow and for contact forces larger than $5g$ charring appears in the wake of the catheter above the electrode. This indicates that the increase in the number of the irrigation pores is not sufficient for the effective cooling for such scenario, hinting that other technologies such as temperature cutoff or variable saline irrigation rates are required.

In terms of lesion size dimensions, the multipore electrode produces lesions comparable to the 6-pore electrodes, and within available experimental data [8].

5.   Limitations

The thermocouples and the minielectrodes are modeled as homogenous without accounting for the interior structure or the impact of the electrical field generated from the minielectrode in the ablation outcome. Nonetheless, a temperature variation is observed at the thermocouples following the tissue and blood temperature rise. Additionally, our model considers constant power ablation protocols with a fixed saline irrigation flow rate and a fixed saline temperature. State-of-the-art catheters use temperature control to titrate the applied power and varying saline irrigation flow rates following the feedback from the thermocouples. The saline temperature also varies according to the irrigation rate [9] and can have an impact in the ablation outcome. These aspects are part of our ongoing work.

References

[1] Petras A, Moreno Weidmann Z, Leoni M, Gerardo-Giorda L, Guerra JM. Systematic characterization of high-power short-duration ablation: Insight from an advanced virtual model. Frontiers in Medical Technology 2021;60.

[2] Petras A, Leoni M, Guerra JM, Jansson J, Gerardo-Giorda L. A computational model of open-irrigated radiofrequency catheter ablation accounting for mechanical properties of the cardiac tissue. International Journal for Numerical Methods in Biomedical Engineering 2019;35(11):e3232.

[3] Guerra JM, Jorge E, Raga S, Gálvez-Montón C, Alonso-Martín C, Rodríguez-Font E, Cinca J, Viñolas X. Effects of open-irrigated radiofrequency ablation catheter design on lesion formation and complications: in vitro comparison of 6 different devices. Journal of Cardiovascular Electrophysiology 2013;24(10):1157–1162.

[4] Finan JD, Fox PM, Morrison B. Non-ideal effects in indentation testing of soft tissues. Biomechanics and Modeling in Mechanobiology 2014;13(3):573–584.

[5] Hasgall P, Di Gennaro F, Baumgartner C, Neufeld E, Lloyd B, Gosselin M, Payne D, Klingenböck A, Kuster N. IT'IS Database for thermal and electromagnetic parameters of biological tissues. itis.swiss/database.

[6] Petras A, Leoni M, Guerra JM, Jansson J, Gerardo-Giorda L. Tissue drives lesion: computational evidence of inter-species variability in cardiac radiofrequency ablation. In International Conference on Functional Imaging and Modeling of the Heart. Springer, 2019; 139–146.

[7] Reddy VY, Grimaldi M, De Potter T, Vijgen JM, Bulava A, Duytschaever MF, Martinek M, Natale A, Knecht S, Neuzil P, et al. Pulmonary vein isolation with very high power, short duration, temperature-controlled lesions: the qdot-fast trial. JACC Clinical Electrophysiology 2019;5(7):778–786.

[8] Kotadia ID, Williams SE, O'Neill M. High-power, short-duration radiofrequency ablation for the treatment of af. Arrhythmia Electrophysiology Review 2019;8(4):265.

[9] Squara F, Maeda S, Aldhoon B, Marginiere J, Santangeli P, Chik WW, Michele J, Zado E, Marchlinski FE. In vitro evaluation of ice-cold saline irrigation during catheter radiofrequency ablation. Journal of Cardiovascular Electrophysiology 2014;25(10):1125–1132.

Address for correspondence:

Argyrios Petras
Altenbergerstrasse 69, 4040 Linz, Austria
argyrios.petras@ricam.oeaw.ac.at